Multifunctional organometallic compounds for the treatment of Chagas Disease: Re(I) tricarbonyl compounds with two different bioactive ligands

Mariano Soba[1,2], Gonzalo Scalese[1], Federico Casuriaga[1], Nicolás Pérez[1], Nicolás Veiga[1], Gustavo A. Echeverría[3], Oscar E. Piro[3], *Ricardo Faccio[4], Leticia Pérez-Díaz[5],* Gilles Gasser[6], *Ignacio Machado[7]*,* Dinorah Gambino[1]*

[1]*Área Química Inorgánica, DEC, Facultad de Química, Universidad de la República, Uruguay*
[2]*Programa de Posgrado en Química, Facultad de Química, Universidad de la República, Montevideo, Uruguay*
[3]*Departamento de Física, Facultad de Ciencias Exactas, Universidad Nacional de La Plata and Institute IFLP (CONICET, CCT-La Plata), La Plata, Argentina*
[4]*Área Física, DETEMA, Facultad de Química, Universidad de la República, Uruguay*
[5]*Laboratorio de Interacciones Moleculares, Facultad de Ciencias, Universidad de la República, Uruguay*
[6]*Chimie ParisTech, PSL University, CNRS, Institute of Chemistry for Life and Health Sciences, Laboratory for Inorganic Chemical Biology, France.*
[7]*Área Química Analítica, DEC, Facultad de Química, Universidad de la República, Uruguay*

* To whom correspondence should be addressed. E-mail: dgambino@fq.edu.uy; imachado@fq.edu.uy Tel. +5982-9249739; fax: +5982-9241906

Table of contents

Fig. S3. (A) ^{1}H-NMR spectra (B) ^{1}H-^{1}H NMR experiments and (C) ^{1}H-^{13}C NMR experiments for *fac*-[Re(I)(CO)$_3$(aminophen)(CTZ)](PF$_6$) complex.

Fig. S4. (A) ^{1}H-NMR spectra (B) ^{1}H-^{1}H NMR experiments and (C) ^{1}H-^{13}C NMR experiments for *fac*-[Re(I)(CO)$_3$(bipy)(CTZ)](PF$_6$) complex.

Fig. S5. (A) ^{1}H-NMR spectra (B) ^{1}H-^{1}H NMR experiments and (C) ^{1}H-^{13}C NMR experiments for *fac*-[Re(I)(CO)$_3$(tmp)(CTZ)](PF$_6$) complex.

Fig. S6. (A) ^{1}H-NMR spectra (B) ^{1}H-^{1}H NMR experiments and (C) ^{1}H-^{13}C NMR experiments for *fac*-[Re(I)(CO)$_3$(dmb)(CTZ)](PF$_6$) complex.

Fig. S7. (A) ^{1}H-NMR spectra (B) ^{1}H-^{1}H NMR experiments and (C) ^{1}H-^{13}C NMR experiments for *fac*-[Re(I)(CO)$_3$(tmp)(KTZ)](PF$_6$) complex.

Fig. S8. Chromatograms obtained in DMSO:fetal bovine serum (50:50) for *fac*-[Re(I)(CO)$_3$(aminophen)(CTZ)](PF$_6$) (a), *fac*-[Re(I)(CO)$_3$(dmb)(CTZ)](PF$_6$) (b) and *fac*-[Re(I)(CO)$_3$(bipy)(CTZ)](PF$_6$) (c). Subscripts 1 and 2 correspond to $t_1 = 0$ and $t_2 = 1$ day, respectively.

Fig. S9. Chromatograms obtained in DMSO:fetal bovine serum (50:50) for *fac*-[Re(I)(CO)$_3$(tmp)(CTZ)](PF$_6$) (d), *fac*-[Re(I)(CO)$_3$(phen)(CTZ)](PF$_6$) (e) and *fac*-[Re(I)(CO)$_3$(tmp)(KTZ)](PF$_6$) (f). Subscripts 1 and 2 correspond to $t_1 = 0$ and $t_2 = 1$ day, respectively.

Fig. S10. Electronic absorption spectra of Re-CTZ-tmp in the absence (black line) and in the presence (color lines) of CT-DNA. The arrow shows the changes upon addition of increasing amount of CT-DNA. (C_{DNA} = 0-20 μM, $C_{complex}$ = 10 μM, samples prepared in DMSO/buffer Tris HCl medium, pH 7.4).

Fig. S11. Fluorescence data obtained for the competitive binding study of [Re(CO)$_3$(tmp)(CTZ)]PF$_6$ to {EB-DNA} adduct (λexc. = 510 nm).

Fig. S12. Docking solutions for *fac*-[Re(I)(CO)$_3$(NN)(CTZ)]$^+$ using CT-DNA as receptor. NN = phen (a), aminophen (b), bipy (c), dmb (d), tmp (e). The solvent-accessible surface is depicted for the receptor, with the interpolated atomic charges mapped on it. The RMSD between the solutions is also depicted. Atom color code: C (grey), N (blue), O (red), Cl (green), H (white).

Fig. S13. Best ranking pose for *fac*-[Re(I)(CO)$_3$(NN)(CTZ)]$^+$ docked into the major groove of CT-DNA. NN = bipy (a), dmb (b), tmp (c). In all cases, the solvent-accessible surface is depicted for the receptor, with the interpolated atomic charges mapped on it. In (d) - (f), the intermolecular interactions between the substrate and the ct-DNA are shown for (a) - (c), respectively. Pi-sigma = C-H-π interaction; conventional = conventional H-bond; Carbon = C-H H-bond. Atom color code: C (grey), N (blue), O (red), Cl (green), H (white).

Fig. S14. a) Intermolecular interactions between the crystalized fluconazole and the receptor, represented as colored dashed lines. Atom color code: C (grey), N (blue), O (red), Cl (green), H (white). b) Redocking results for fluconazole. The crystallized fluconazole molecule is superimposed in green.

Table S1. Crystal data and structure refinement for the triclinic and monoclinic polymorphs of *fac*-[Re(I)(CO)$_3$(phen)(CTZ)](PF$_6$).

Polymorph	**Triclinic**	**Monoclinic**
Empirical formula	$C_{37}H_{25}ClF_6N_4O_3PRe$	$C_{37}H_{25}ClF_6N_4O_3PRe$
Formula weight	940.23	940.23
Temperature (K)	297(2)	297(2)
Wavelength (Å)	0.71073	0.71073
Crystal system	Triclinic	Monoclinic
Space group	P-1	$P2_1/n$
Unit cell dimensions		
a (Å)	11.3683(3)	19.2076(6)
b (Å)	12.1500(3)	11.9631(3)
c (Å)	14.2904(4)	32.482(1)
α (º)	110.797(2)	90.000
β (º)	99.919(2)	104.958(4)
γ (º)	103.574(2)	90.000
Volume (Å^3)	1721.30(8)	7211.0(4)
Z, calc. density (Mg/m^3)	2, 1.814	8, 1.732
Absorption coeff. (mm-1)	3.731	3.563
F(000)	920	3680
Crystal size (mm^3)	0.440 x 0.407 x 0.200	0.472 x 0.252 x 0.143
ϑ-range for data collect. (º)	3.363 to 29.023	2.979 to 26.000
Index ranges	-15≤h≤15, -16≤k≤15, -17≤l≤17	-23≤h≤13, -14≤k≤14, -33≤l≤39
Reflections collected	16130	36391
Independent reflections	7486 [R(int) = 0.0316]	14104 [R(int) = 0.0343]
Obs. reflections [I>2σ(I)]	6540	10770
Completeness (%)	99.7 (to ϑ = 25.242°)	99.8 (to ϑ = 25.242°)
Refinement method	Full-matrix least-squares on F^2	Full-matrix least-squares on F^2
Data / restraints / parameters	7486 / 7 / 431	14104 / 0 / 955
Goodness-of-fit on F^2	1.046	1.138
Final R indices[a] [I>2σ(I)]	R1 = 0.0292, wR2 = 0.0599	R1 = 0.0403, wR2 = 0.0728
R indices (all data)	R1 = 0.0375, wR2 = 0.0632	R1 = 0.0631, wR2 = 0.0855
Larg. diff. peak & hole (e.Å^{-3})	1.015 and -0.912	0.996 and -1.924

[a] $R_1=\Sigma||F_o|-|F_c||/\Sigma|F_o|$, $wR_2=[\Sigma w(|F_o|^2-|F_c|^2)^2/\Sigma w(|F_o|^2)^2]^{1/2}$

Table S2. Gradient conditions for RP-HPLC-DAD analysis.

Time (min)	A (%)	B (%)
0 – 3	100	0
3 – 6	100 – 75	0 – 25
6 – 9	75 – 66	25 – 34
9 – 20	66 – 0	34 – 100
20 – 27	0	100
27 – 30	0 – 100	100 – 0

Table S3a. Bond lengths [Å] and angles [°] around the metal in $[Re(I)(CO)_3(phen)(CTZ)]$ complex of *fac*-$[Re(I)(CO)_3(phen)(CTZ)](PF_6)$ triclinic polymorph.

C(1)-Re	1.923(4)	C(3)-Re-N(2A)	171.7(1)
C(2)-Re	1.900(4)	C(1)-Re-N(2A)	93.0(1)
C(3)-Re	1.924(4)	C(2)-Re-N(2B)	171.3(1)
N(1A)-Re	2.190(3)	C(3)-Re-N(2B)	96.3(2)
N(2A)-Re	2.171(3)	C(1)-Re-N(2B)	98.2(1)
N(2B)-Re	2.179(3)	N(2A)-Re-N(2B)	75.4(1)
		C(2)-Re-N(1A)	90.7(1)
C(2)-Re-C(3)	89.3(2)	C(3)-Re-N(1A)	95.0(1)
C(2)-Re-C(1)	88.5(2)	C(1)-Re-N(1A)	176.6(1)
C(3)-Re-C(1)	88.3(2)	N(2A)-Re-N(1A)	83.88(9)
C(2)-Re-N(2A)	98.9(1)	N(2B)-Re-N(1A)	82.3(1)

Table S3b. Bond lengths [Å] and angles [°] around the metal in the two $[Re(I)(CO)_3(phen)(CTZ)]$ conformers of *fac*-$[Re(I)(CO)_3(phen)(CTZ)](PF_6)$ monoclinic polymorph.

Conformer 1		**Conformer 2**	
C(11)-Re(1)	1.907(6)	C(21)-Re(2)	1.900(6)
C(12)-Re(1)	1.908(6)	C(22)-Re(2)	1.923(6)
C(13)-Re(1)	1.924(6)	C(23)-Re(2)	1.919(6)
N(11A)-Re(1)	2.183(4)	N(21A)-Re(2)	2.177(4)
N(12A)-Re(1)	2.175(4)	N(22A)-Re(2)	2.178(4)
N(12B)-Re(1)	2.177(4)	N(22B)-Re(2)	2.179(4)
C(11)-Re(1)-C(12)	86.6(2)	C(21)-Re(2)-C(22)	86.9(2)
C(11)-Re(1)-C(13)	89.4(2)	C(21)-Re(2)-C(23)	87.4(2)
C(12)-Re(1)-C(13)	87.1(2)	C(22)-Re(2)-C(23)	88.1(2)
C(11)-Re(1)-N(12A)	92.1(2)	C(21)-Re(2)-N(22A)	95.8(2)
C(12)-Re(1)-N(12A)	99.9(2)	C(22)-Re(2)-N(22A)	97.8(2)
C(13)-Re(1)-N(12A)	172.9(2)	C(23)-Re(2)-N(22A)	173.3(2)
C(11)-Re(1)-N(12B)	98.7(2)	C(21)-Re(2)-N(22B)	93.6(2)
C(12)-Re(1)-N(12B)	173.1(2)	C(22)-Re(2)-N(22B)	173.3(2)
C(13)-Re(1)-N(12B)	97.3(2)	C(23)-Re(2)-N(22B)	98.5(2)
N(12A)-Re(1)-N(12B)	75.6(2)	N(22A)-Re(2)-N(22B)	75.5(2)
C(11)-Re(1)-N(11A)	175.5(2)	C(21)-Re(2)-N(21A)	178.2(2)
C(12)-Re(1)-N(11A)	92.2(2)	C(22)-Re(2)-N(21A)	93.8(2)
C(13)-Re(1)-N(11A)	94.9(2)	C(23)-Re(2)-N(21A)	94.2(2)
N(12A)-Re(1)-N(11A)	83.8(2)	N(22A)-Re(2)-N(21A)	82.5(2)
N(12B)-Re(1)-N(11A)	82.2(2)	N(22B)-Re(2)-N(21A)	85.5(2)

Table S4. Integrated area of HPLC peaks for the analysis of *fac*-[Re(I)(CO)$_3$(NN)(CTZ)](PF$_6$) compounds and caffeine (internal standard) after different times of incubation with human plasma (t in hours).

Compound	**A $_{Compound}$**	**A $_{Caffein}$ (t_R = 3.159)**	**A $_{Compound}$/A $_{Caffein}$**
Blank t=0	-	460.37	-
Blank t=24	-	12.65	-
***fac*-[Re(I)(CO)$_3$(tmp)(CTZ)](PF$_6$) (t_R = 2.599)**			
t=0	718.15	716.12	1.0
t=1	620.40	620.92	1.0
t=3	583.81	525.19	1.1
t=6	423.42	373.48	1.1
t=24	344.10	382.26	0.9
***fac*-[Re(I)(CO)$_3$(dmb)(CTZ)](PF$_6$) (t_R = 1.838)**			
t=0	374.67	426.74	0.9
t=1	275.11	225.67	1.2
t=3	288.95	258.31	1.1
t=6	429.38	344.59	1.2
t=24	292.39	263.15	1.1
***fac*-[Re(I)(CO)$_3$(bipy)(CTZ)](PF$_6$) (t_R = 1.778)**			
t=0	431.89	400.43	1.1
t=1	426.02	421.83	1.0
t=3	456.18	480.07	1.0
t=6	519.30	428.57	1.2
t=24	420.12	381.68	1.1
***fac*-[Re(I)(CO)$_3$(phen)(CTZ)](PF$_6$) (t_R = 1.774)**			
t=0	393.10	394.55	1.0
t=1	284.25	242.26	1.2
t=3	754.83	554.74	1.4
t=6	545.46	458.02	1.2
t=24	314.31	292.41	1.1
***fac*-[Re(I)(CO)$_3$(amino)(CTZ)](PF$_6$) (t_R = 1.745)**			
t=0	354.63	406.65	0.9
t=1	288.59	393.05	0.7
t=3	121.97	174.36	0.7
t=6	247.62	332.45	0.7
t=24	377.81	477.84	0.8
***fac*-[Re(I)(CO)$_3$(tmp)(KTZ)](PF$_6$) (t_R = 1.791)**			
t=0	811.75	299.05	3.0

t=1	1059.71	321.89	3.3
t=3	576.42 256.38 (peak 2)	367.31	**1.6***
t=6	536.04 256.71 (peak 2)	292.11	**1.8***
t=24	628.32 656.40 (peak 2)	462.74	**1.4***
CTZ (t_R = 2.047)			
t=0	19.5	403.39	0.05
t=1	21.2	468.87	0.05
t=3	18.7	366.52	0.05
t=6	15.3	276.71	0.06
t=24	16.7	279.93	0.06

(*): shows the incubation times where the compound started to decompose, as demonstrated by the diminution of the main peak area, and the appearance of a 2nd peak. A = area under the peak.

Table S5. Molecular docking results.

Receptor	Substrate	Chemscore	ΔG_{bind} (kJ/mol)[a]	Chemscore terms[b]			
				H-bonds	Lipophilic interactions	entropic loss	Clash
CT-DNA	$[Re(CO)_3(phen)(CTZ)]^+$	17.5	-17.5	1.98	74.7	1.29	0.04
	$[Re(CO)_3(aminophen)(CTZ)]^+$	18.7	-18.9	2.89	61.5	1.36	0.00
	$[Re(CO)_3(bipy)(CTZ)]^+$	17.5	-17.7	1.99	76.1	1.30	0.04
	$[Re(CO)_3(dmb)(CTZ)]^+$	18.0	-18.2	1.99	79.4	1.27	0.17
	$[Re(CO)_3(tmp)(CTZ)]^+$	17.7	-18.0	1.98	77.6	1.23	0.16
lanosterol 14-α-demethylase (*T. cruzi*)	CTZ	44.6	-52.2	0.00	376.9	1.33	0.24
	$[Re(CO)_3(tmp)(CTZ)]^+$	39.4	-73.6	0.00	608.9	1.23	24.1

[a] Estimated by the chemscore scoring function. [b] Chemscore energy terms: receptor-substrate hydrogen bond, lipophilic interactions, entropic loss upon binding, clash penalty and internal ligand strain.

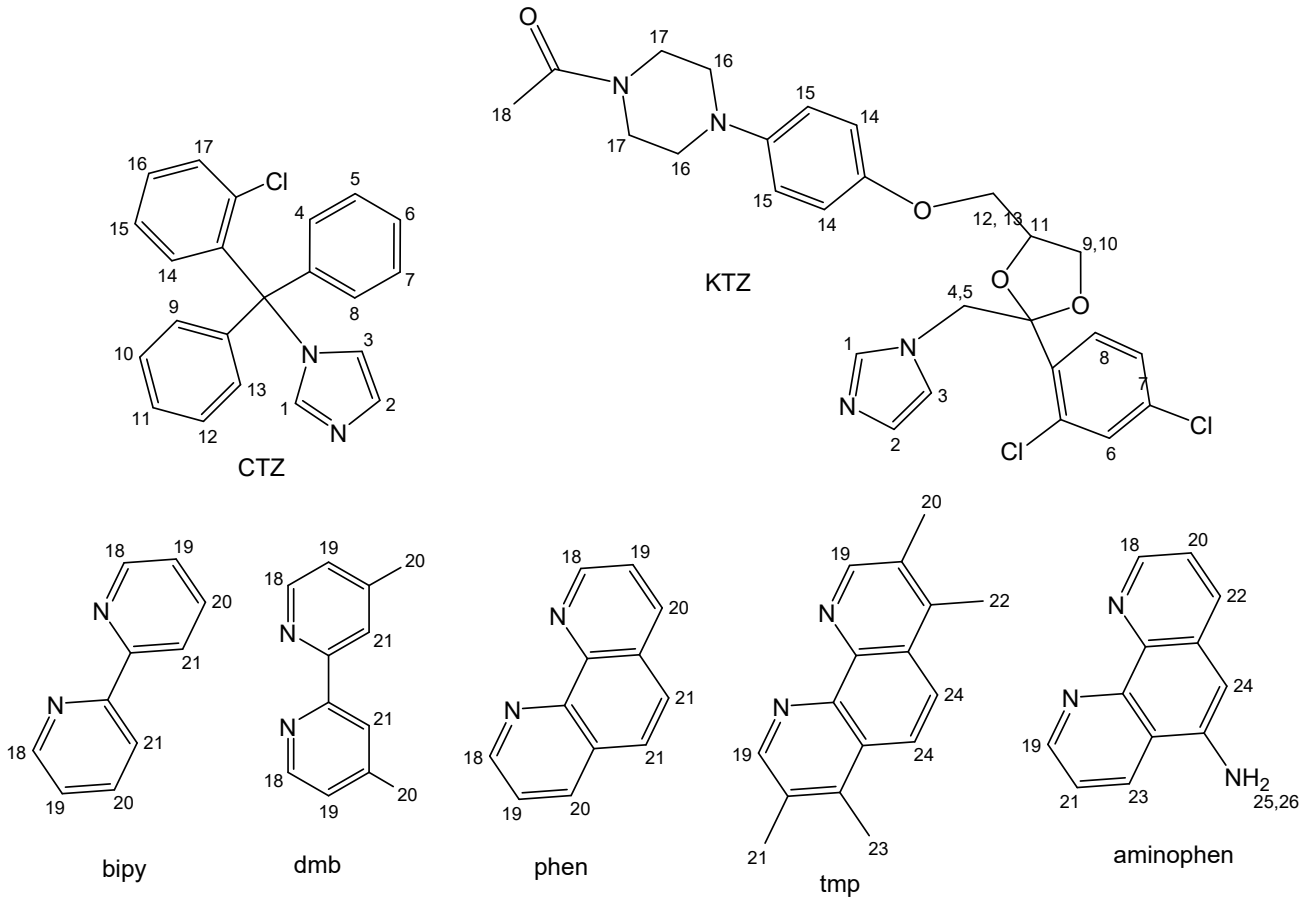

Fig S1. Numbering scheme of the ligands for ^{1}H-NMR assignment.

(A) ^{1}H-RMN

***fac*-[Re(I)(CO)$_3$(phen)(CTZ)](PF$_6$)**

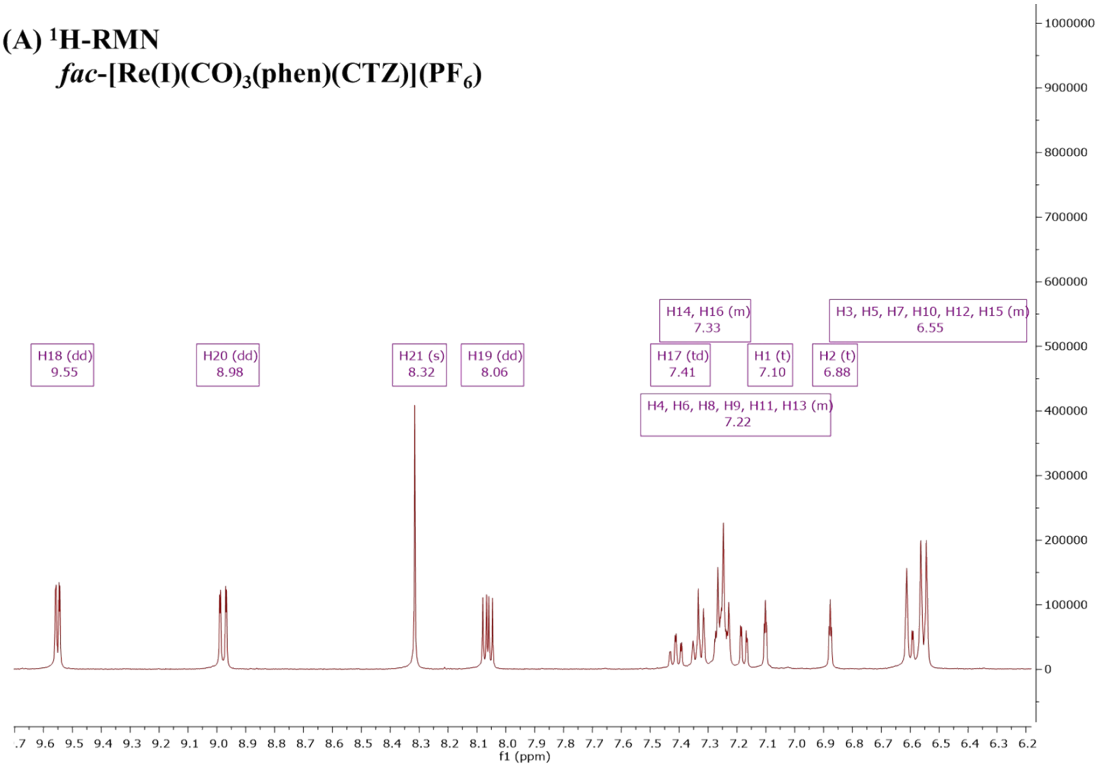

(B) ^{1}H-^{1}H- COSY

***fac*-[Re(I)(CO)$_3$(phen)(CTZ)](PF$_6$)**

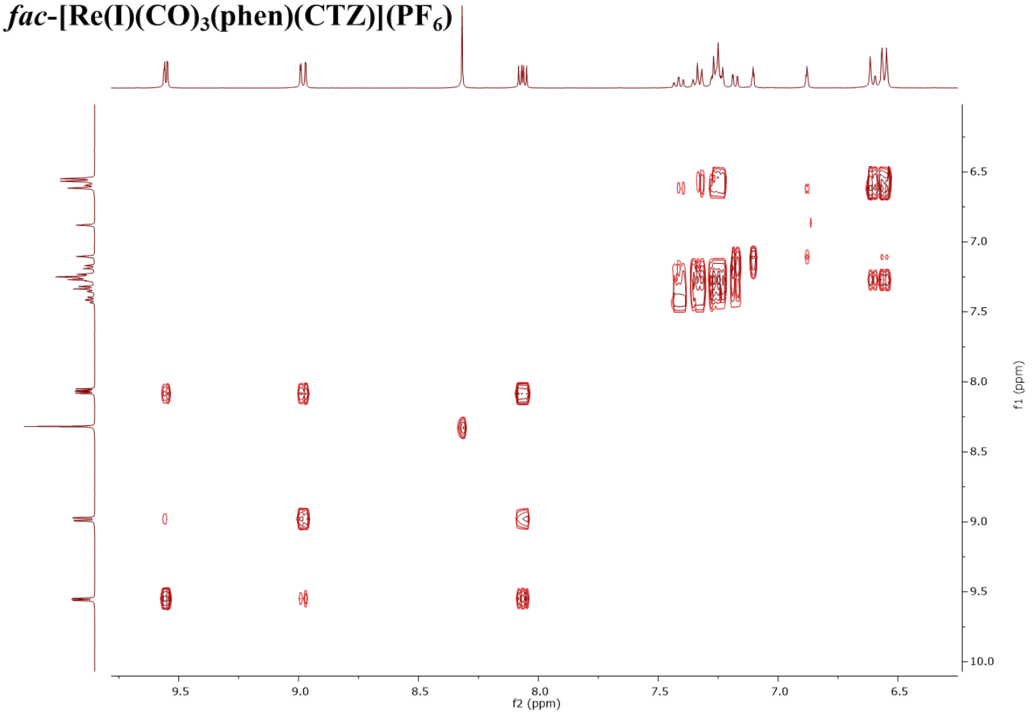

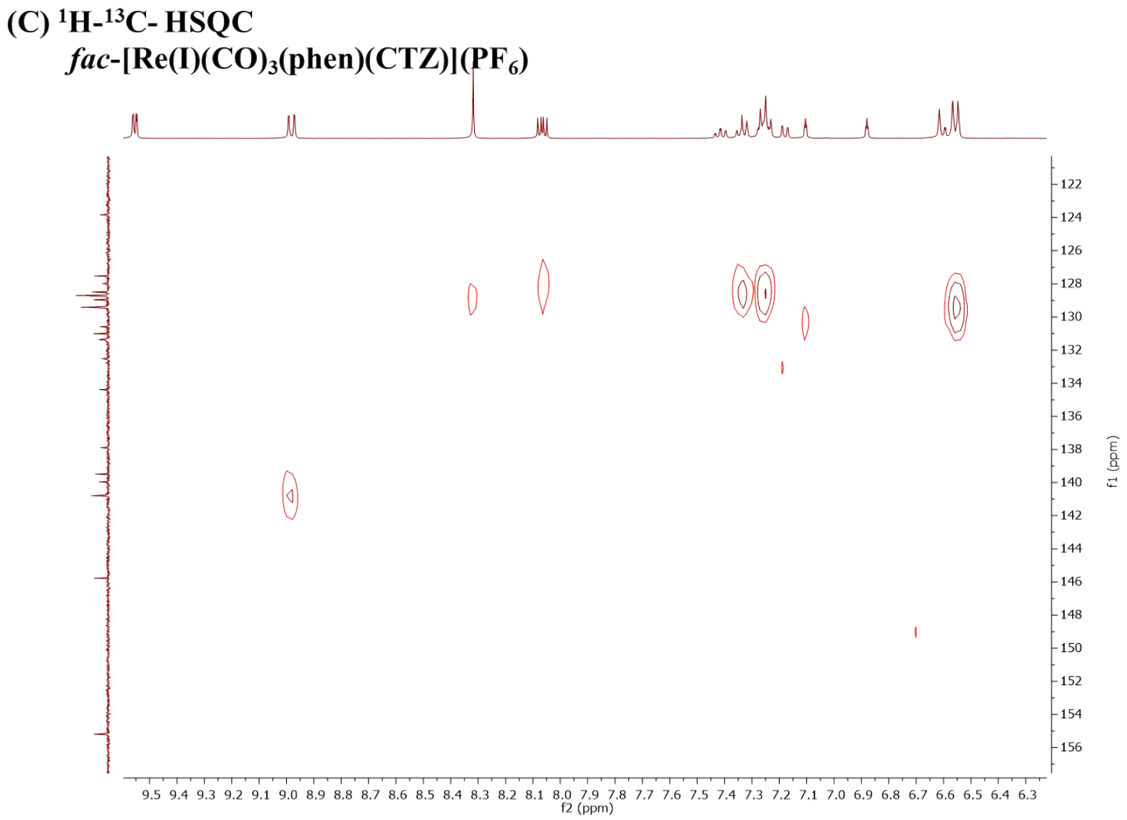

Fig. S2. (A) ^{1}H-NMR spectra (B) ^{1}H-^{1}H NMR experiments and (C) ^{1}H-^{13}C NMR experiments for *fac*-[Re(I)(CO)$_3$(phen)(CTZ)](PF$_6$) complex.

(A) ^{1}H-RMN

***fac*-[Re(I)(CO)$_3$(aminophen)(CTZ)](PF$_6$)**

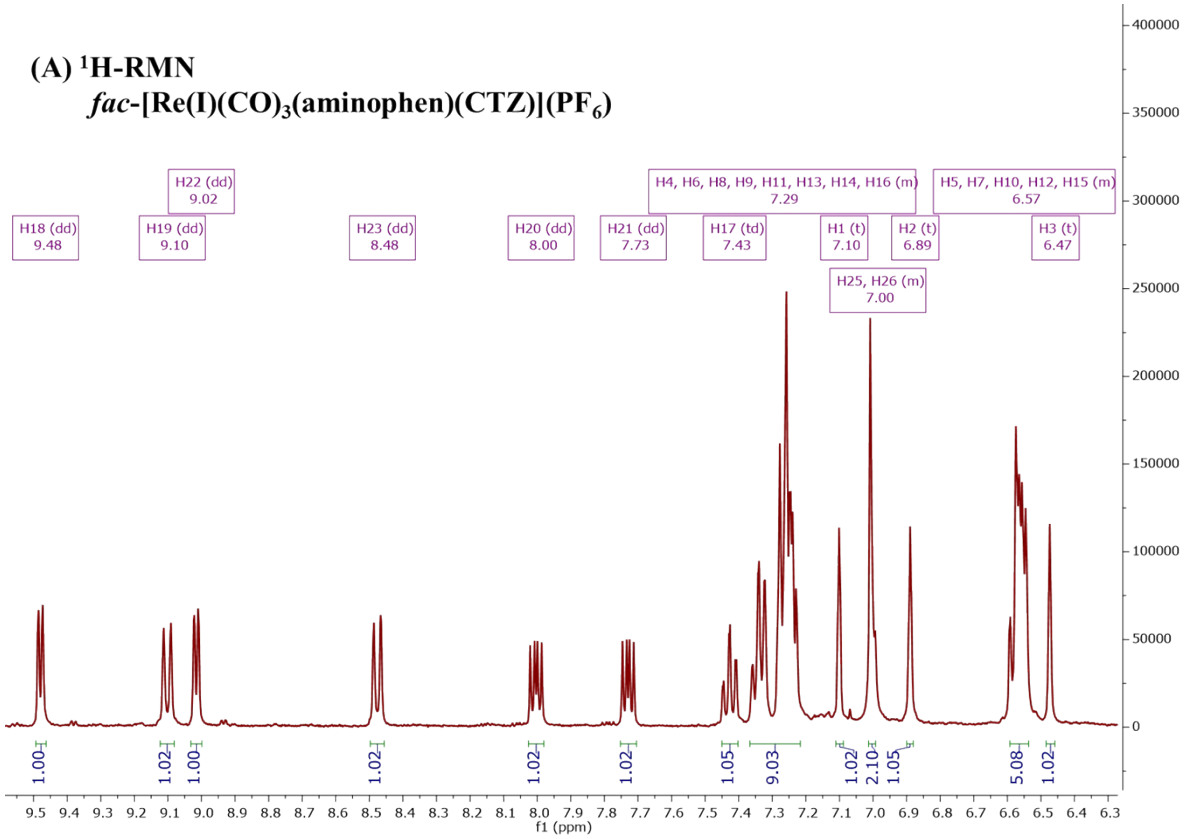

(B) ^{1}H-^{1}H- COSY

***fac*-[Re(I)(CO)$_3$(aminophen)(CTZ)](PF$_6$)**

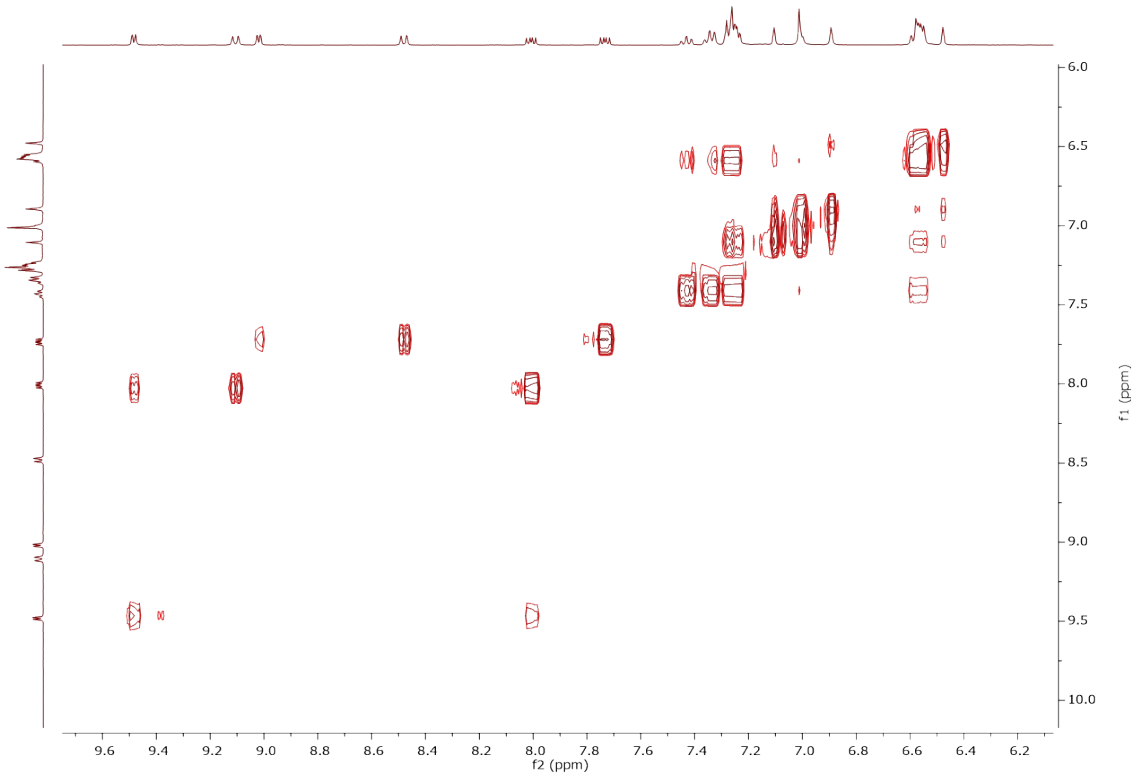

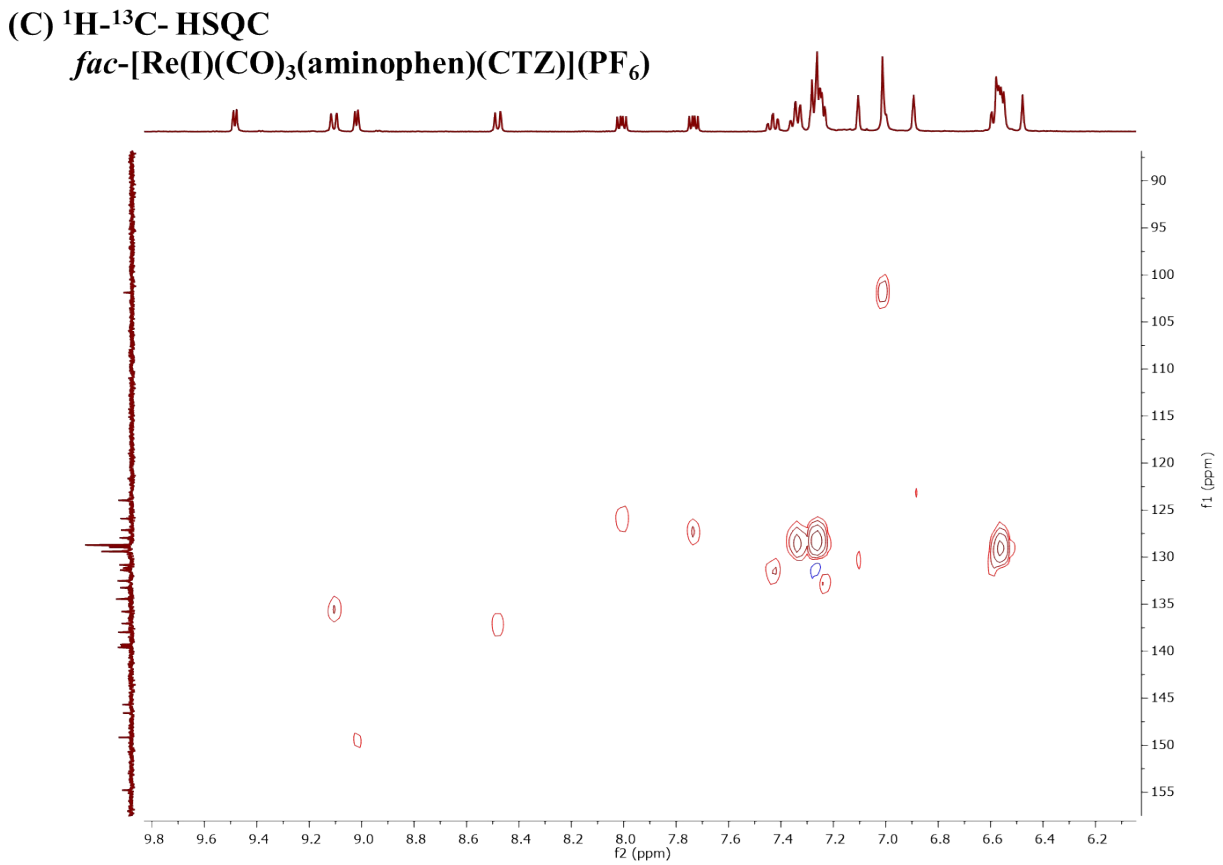

Fig. S3. (A) ^{1}H-NMR spectra (B) ^{1}H-^{1}H NMR experiments and (C) ^{1}H-^{13}C NMR experiments for *fac*-[Re(I)(CO)$_3$(aminophen)(CTZ)](PF$_6$) complex.

(A) ^{1}H-RMN

***fac*-[Re(I)(CO)$_3$(bipy)(CTZ)](PF$_6$)**

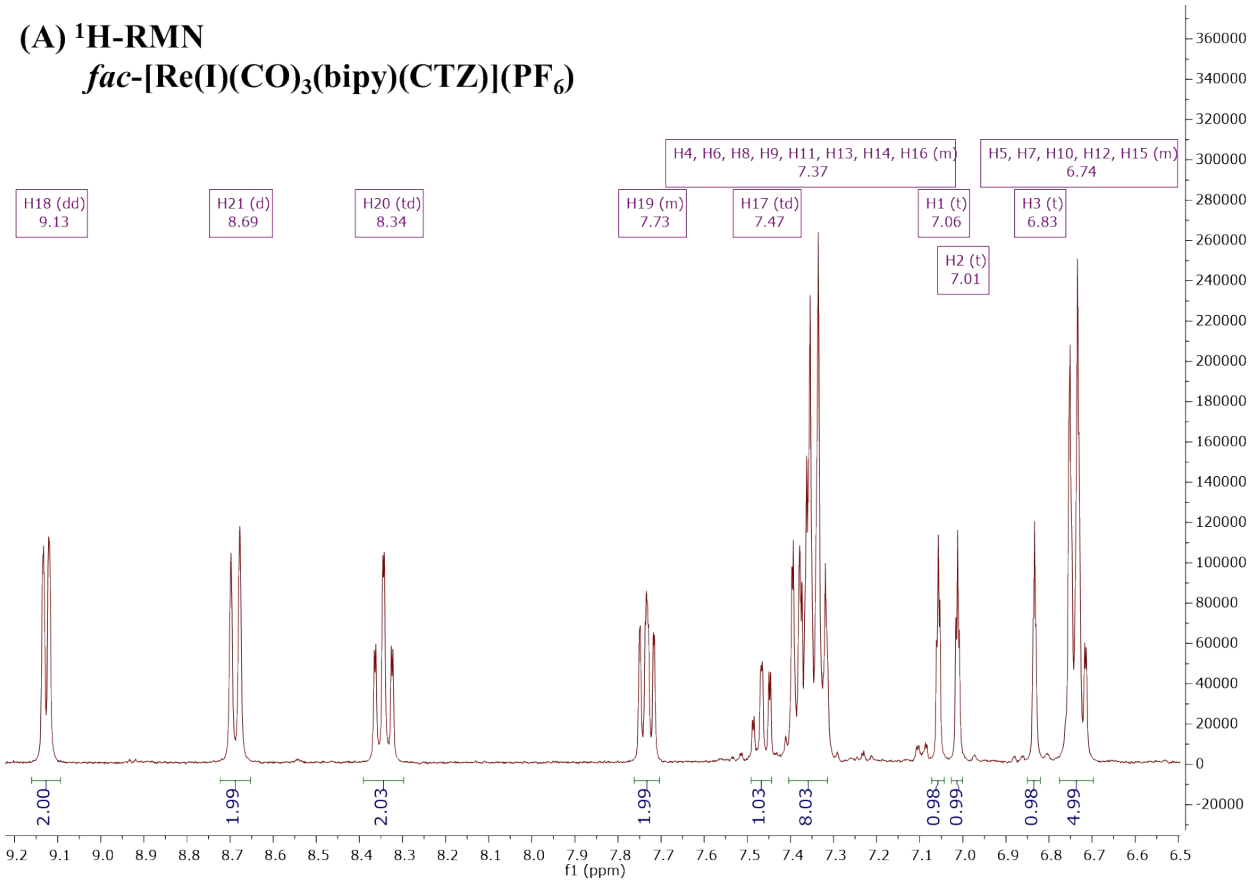

(B) ^{1}H-^{1}H- COSY

***fac*-[Re(I)(CO)$_3$(bipy)(CTZ)](PF$_6$)**

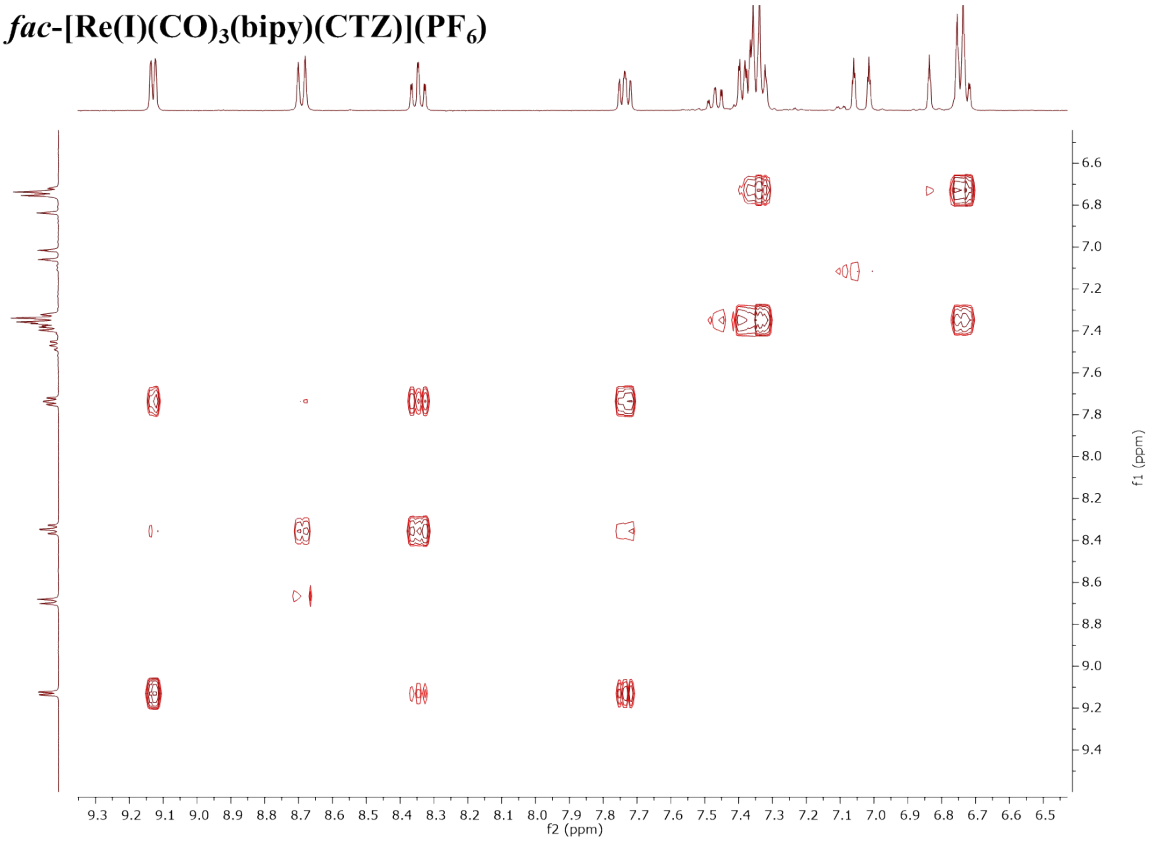

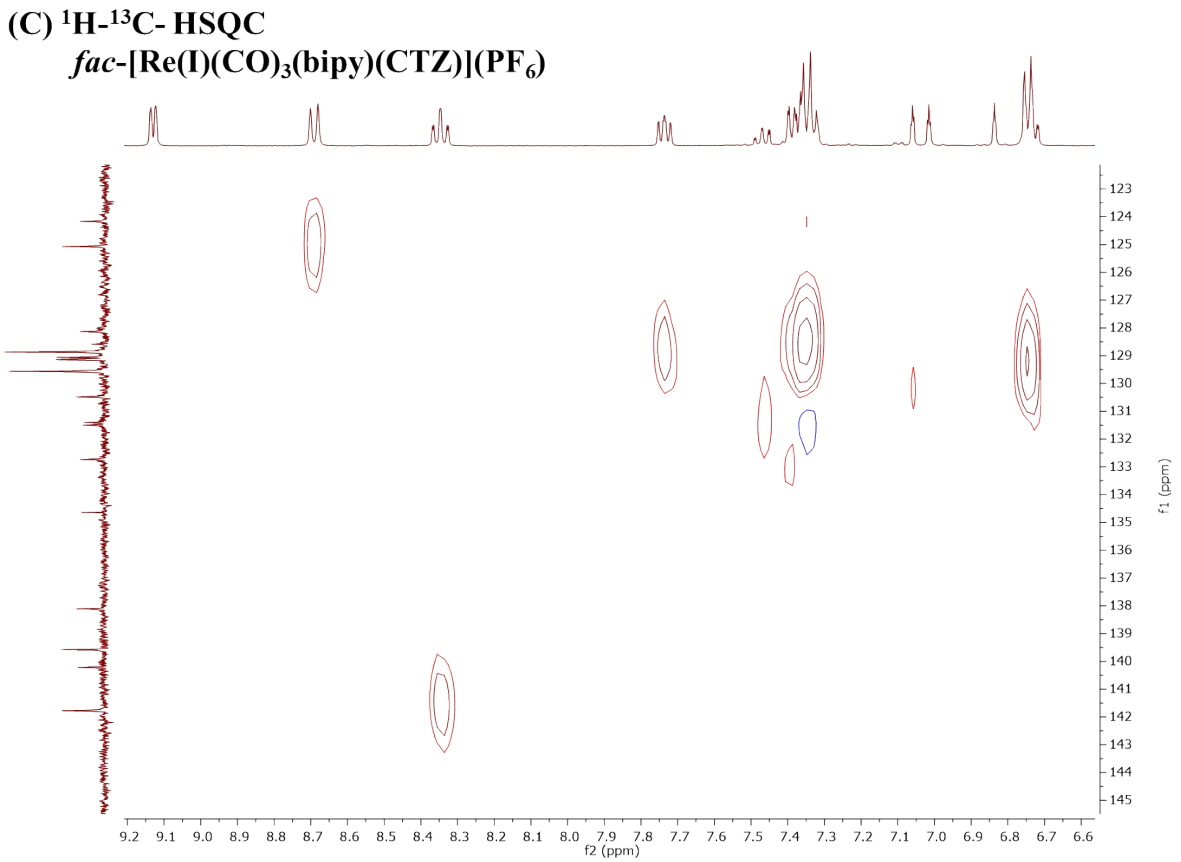

Fig. S4. (A) ^{1}H-NMR spectra (B) ^{1}H-^{1}H NMR experiments and (C) ^{1}H-^{13}C NMR experiments for *fac*-[Re(I)(CO)$_3$(bipy)(CTZ)](PF$_6$) complex.

(A) ^{1}H-NMR

***fac*-[Re(I)(CO)$_3$(tmp)(CTZ)](PF$_6$)**

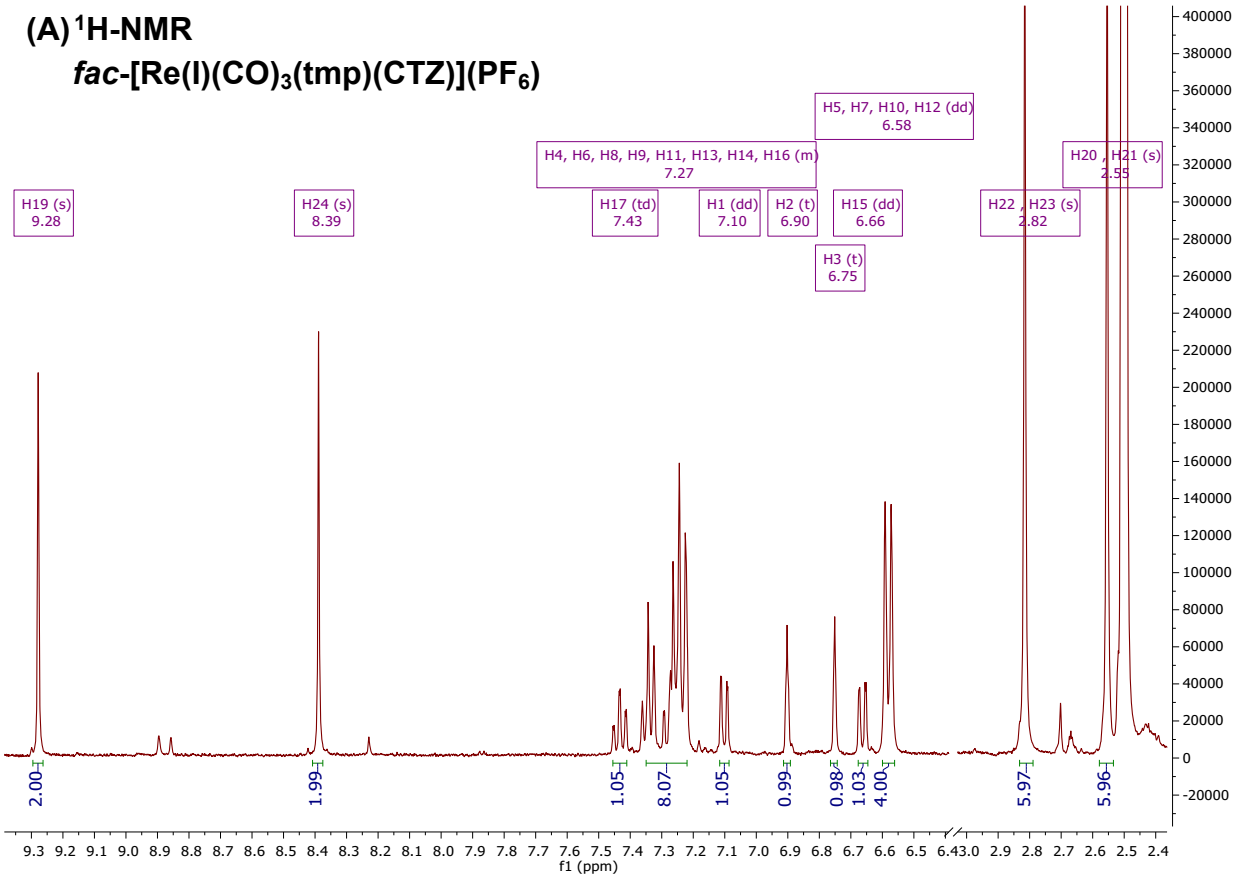

(B) ^{1}H-^{1}H- COSY

***fac*-[Re(I)(CO)$_3$(tmp)(CTZ)](PF$_6$)**

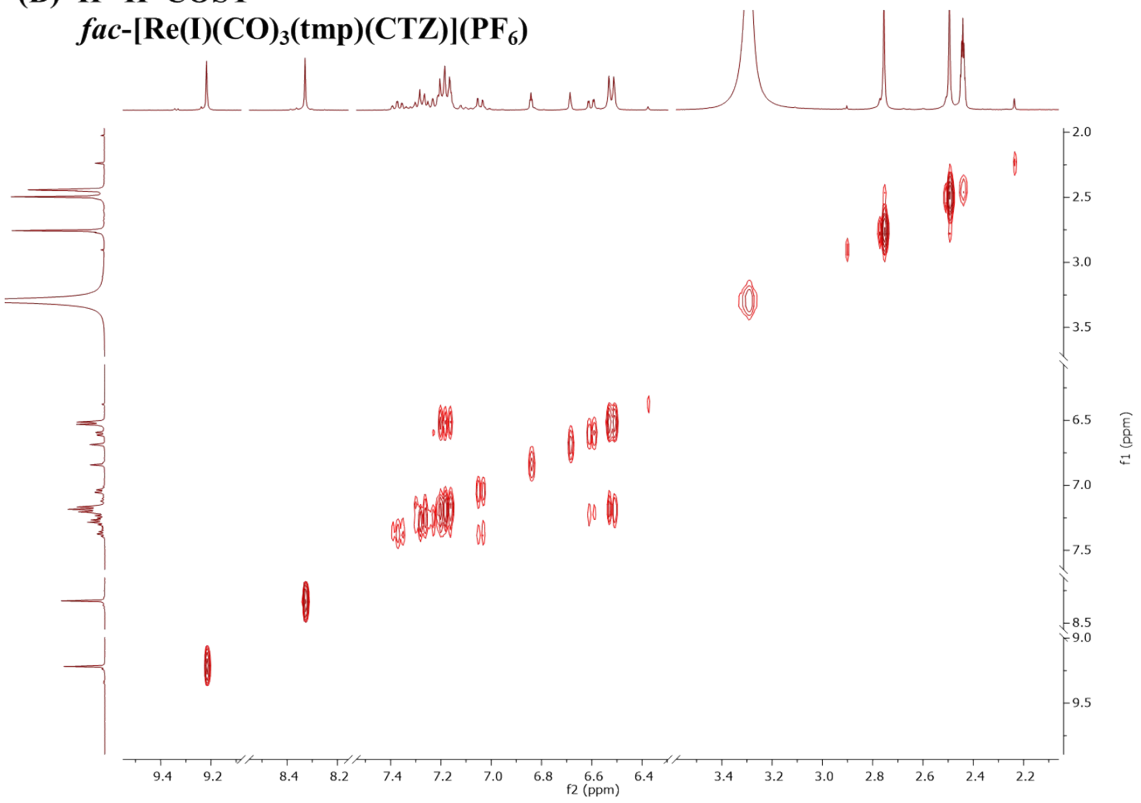

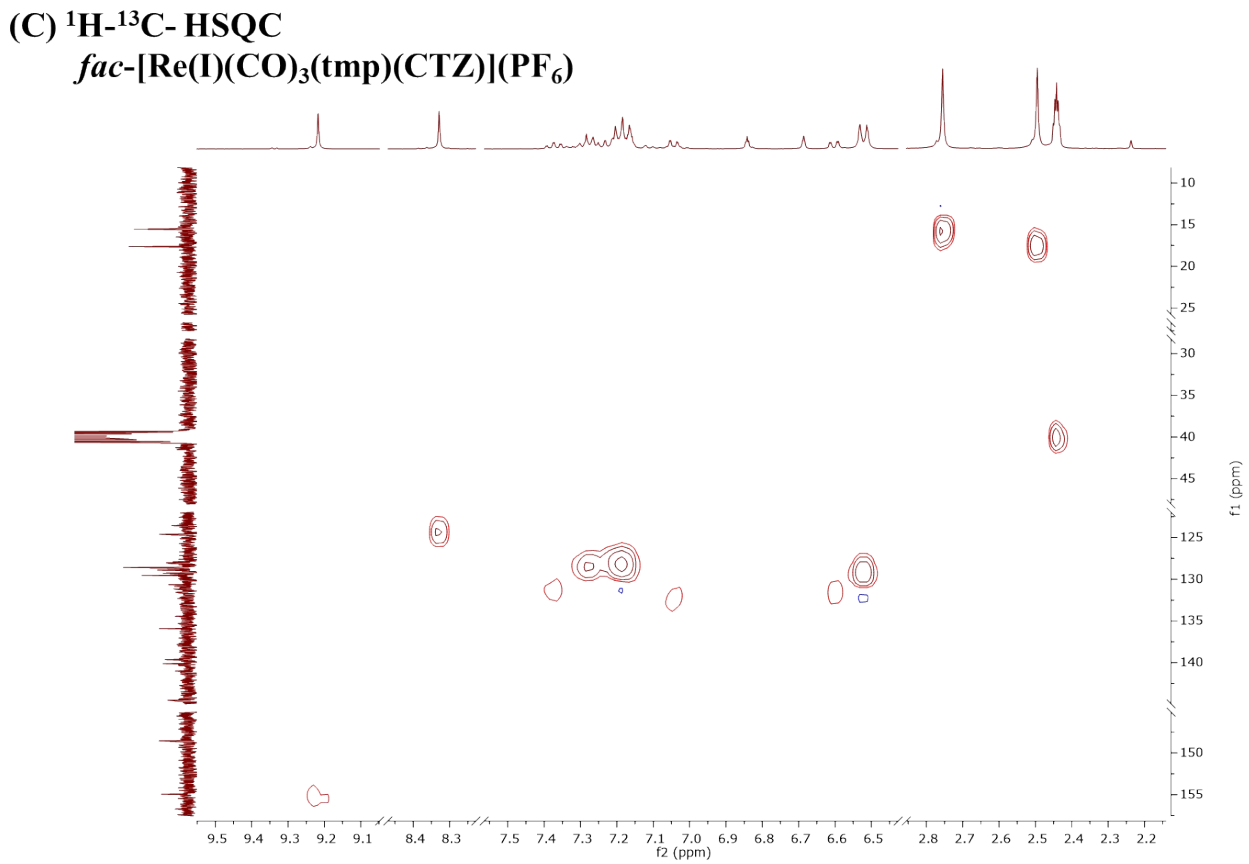

Fig. S5. (A) ^{1}H-NMR spectra (B) ^{1}H-^{1}H NMR experiments and (C) ^{1}H-^{13}C NMR experiments for *fac*-[Re(I)(CO)$_3$(tmp)(CTZ)](PF$_6$) complex.

(A) ^{1}H-RMN

***fac*-[Re(I)(CO)$_3$(dmb)(CTZ)](PF$_6$)**

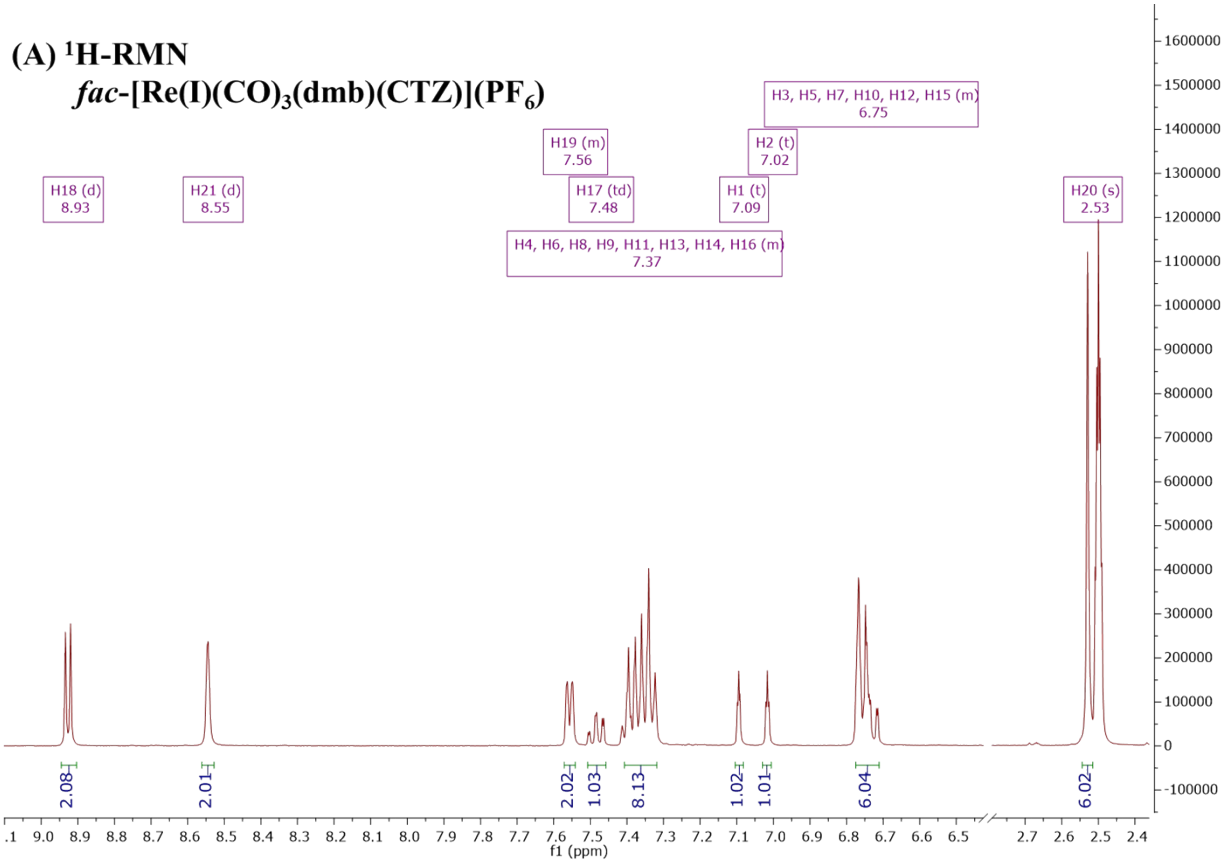

(B) ^{1}H-^{1}H- COSY

***fac*-[Re(I)(CO)$_3$(dmb)(CTZ)](PF$_6$)**

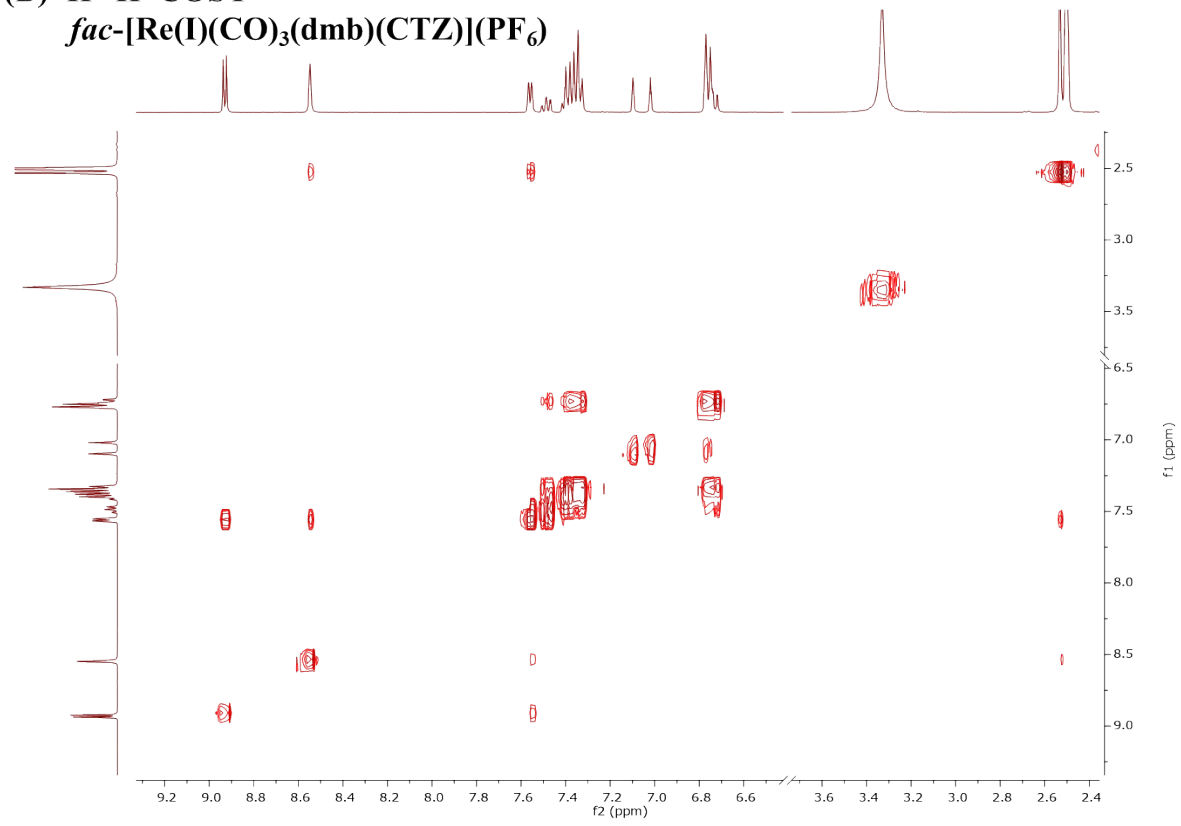

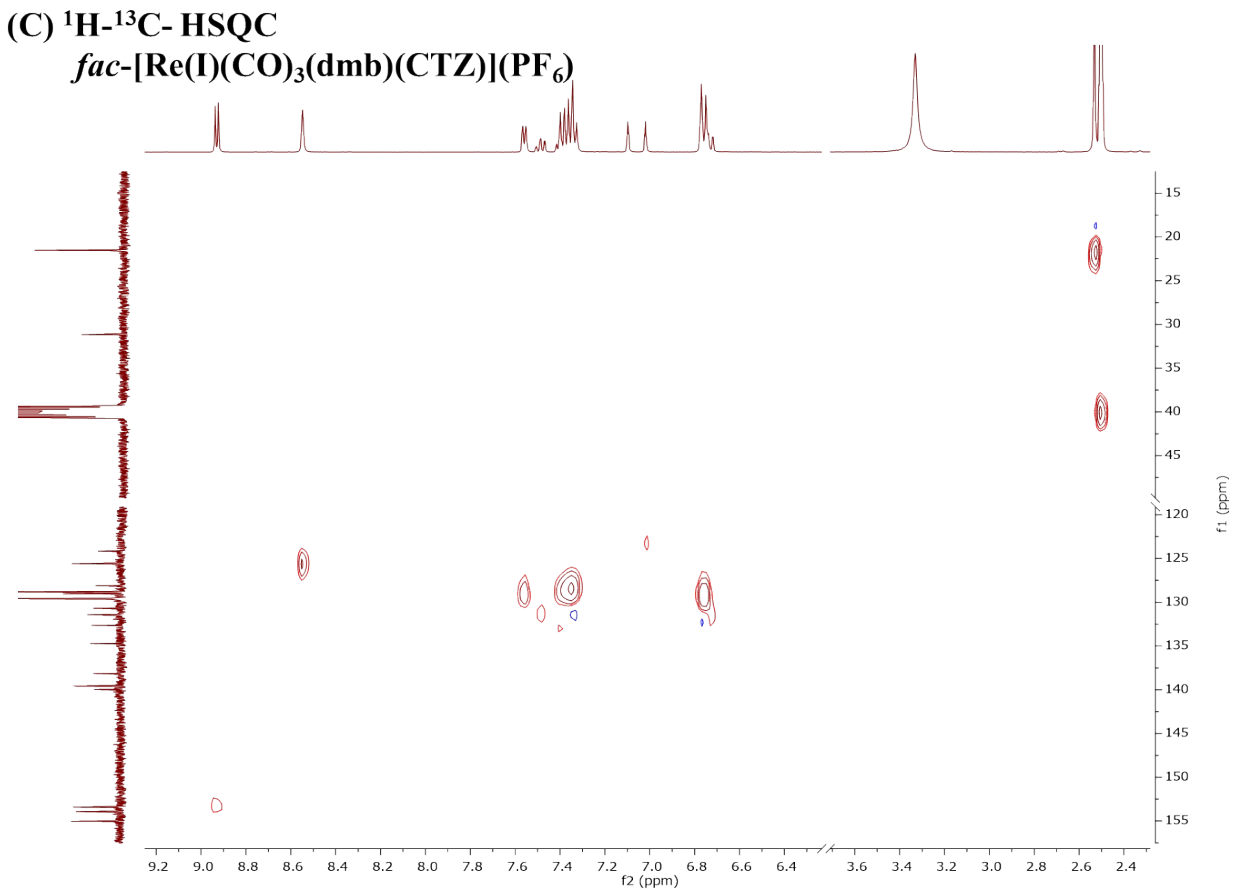

Fig. S6. (A) ^{1}H-NMR spectra (B) ^{1}H-^{1}H NMR experiments and (C) ^{1}H-^{13}C NMR experiments for *fac*-[Re(I)(CO)$_3$(dmb)(CTZ)](PF$_6$) complex.

(A) ^{1}H-RMN

***fac*-[Re(I)(CO)$_3$(tmp)(KTZ)](PF$_6$)**

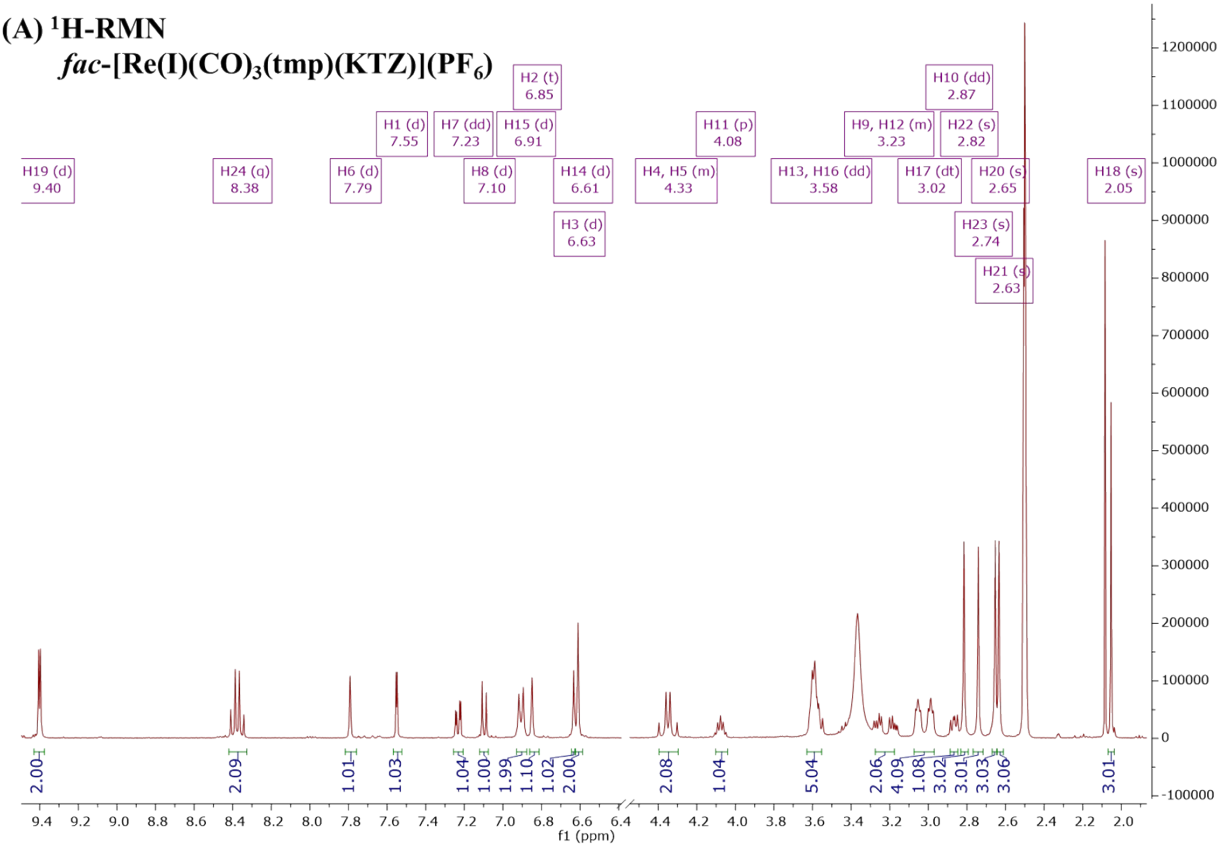

(B) ^{1}H-^{1}H- COSY

***fac*-[Re(I)(CO)$_3$(tmp)(KTZ)](PF$_6$)**

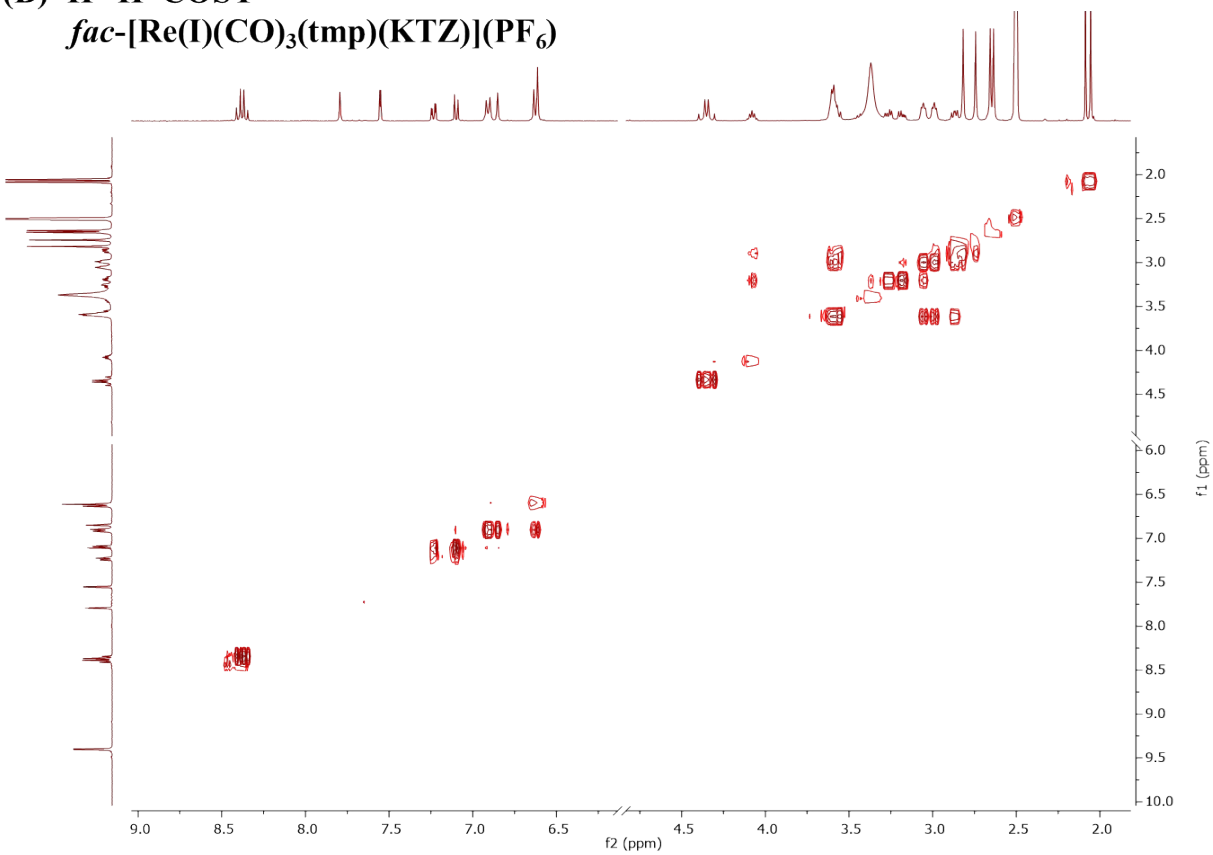

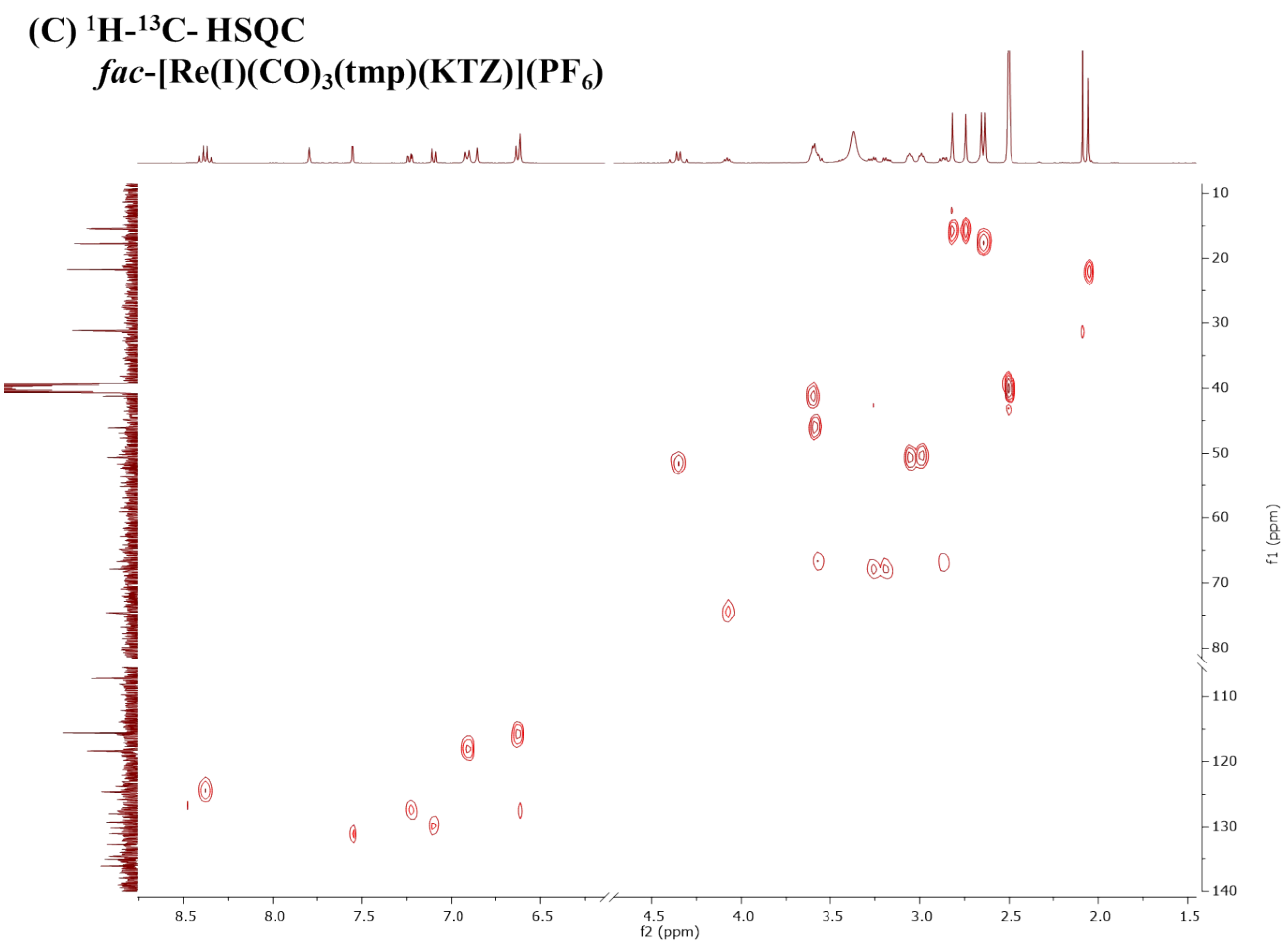

Fig. S7. (A) ^{1}H-NMR spectra (B) ^{1}H-^{1}H NMR experiments and (C) ^{1}H-^{13}C NMR experiments for *fac*-[Re(I)(CO)$_3$(tmp)(KTZ)](PF$_6$) complex.

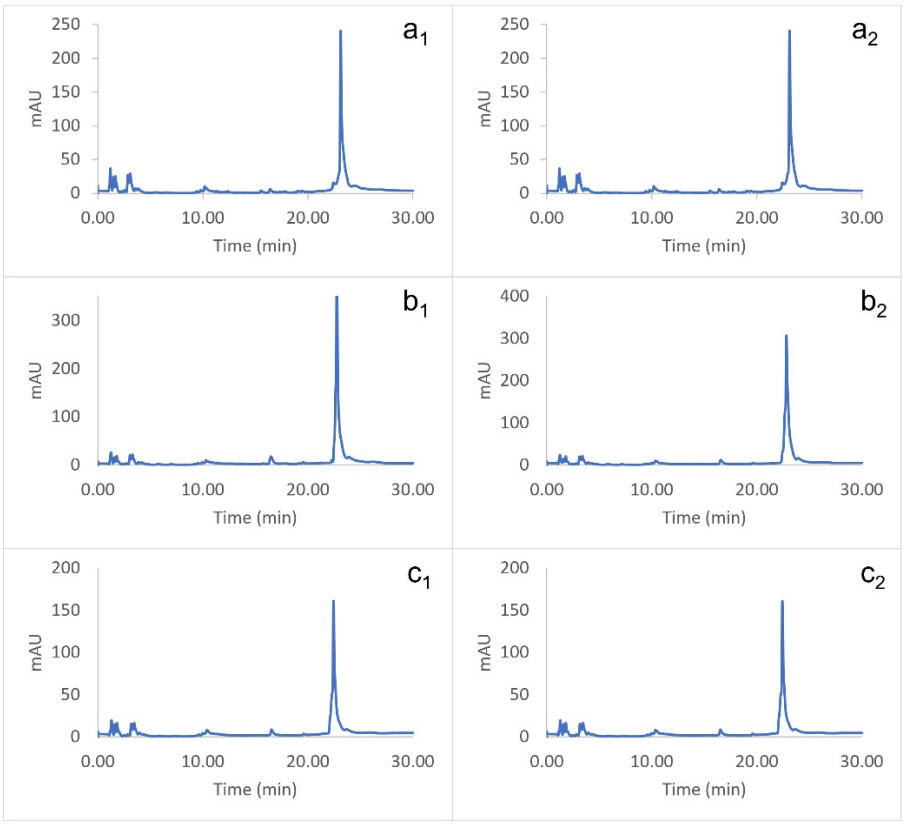

Fig. S8. Chromatograms obtained in DMSO:fetal bovine serum (50:50) for *fac*-[Re(I)(CO)$_3$(aminophen)(CTZ)](PF$_6$) (a), *fac*-[Re(I)(CO)$_3$(dmb)(CTZ)](PF$_6$) (b) and *fac*-[Re(I)(CO)$_3$(bipy)(CTZ)](PF$_6$) (c). Subscripts 1 and 2 correspond to $t_1 = 0$ and $t_2 = 1$ day, respectively.

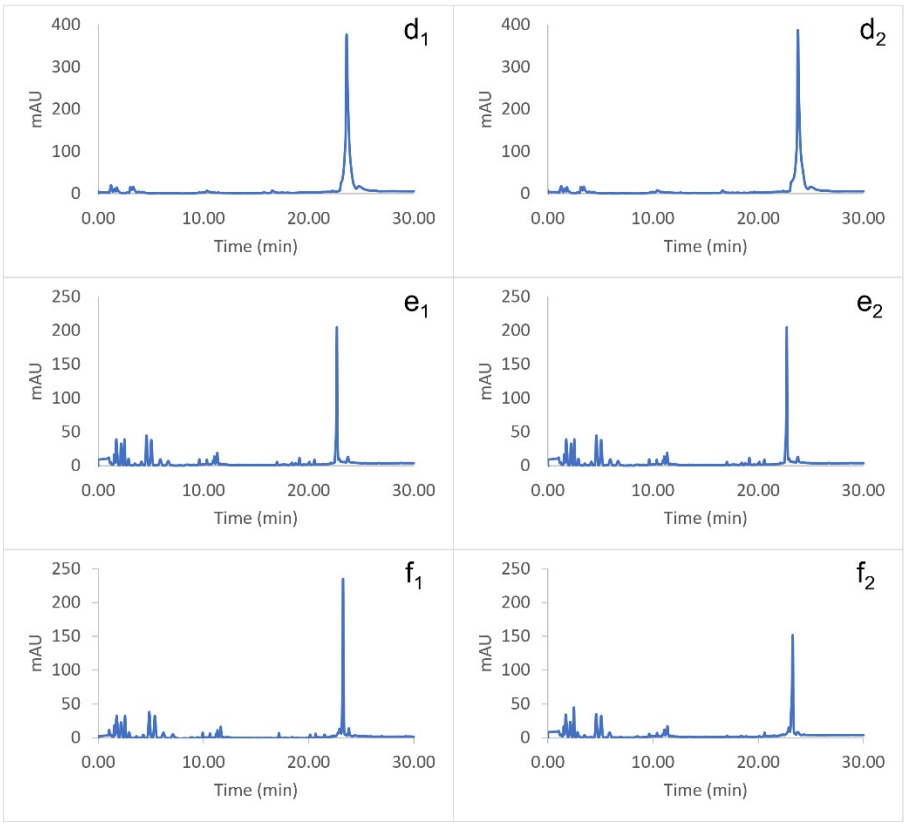

Fig. S9. Chromatograms obtained in DMSO:fetal bovine serum (50:50) for *fac*-[Re(I)(CO)$_3$(tmp)(CTZ)](PF$_6$) (d), *fac*-[Re(I)(CO)$_3$(phen)(CTZ)](PF$_6$) (e) and *fac*-[Re(I)(CO)$_3$(tmp)(KTZ)](PF$_6$) (f). Subscripts 1 and 2 correspond to $t_1 = 0$ and $t_2 = 1$ day, respectively.

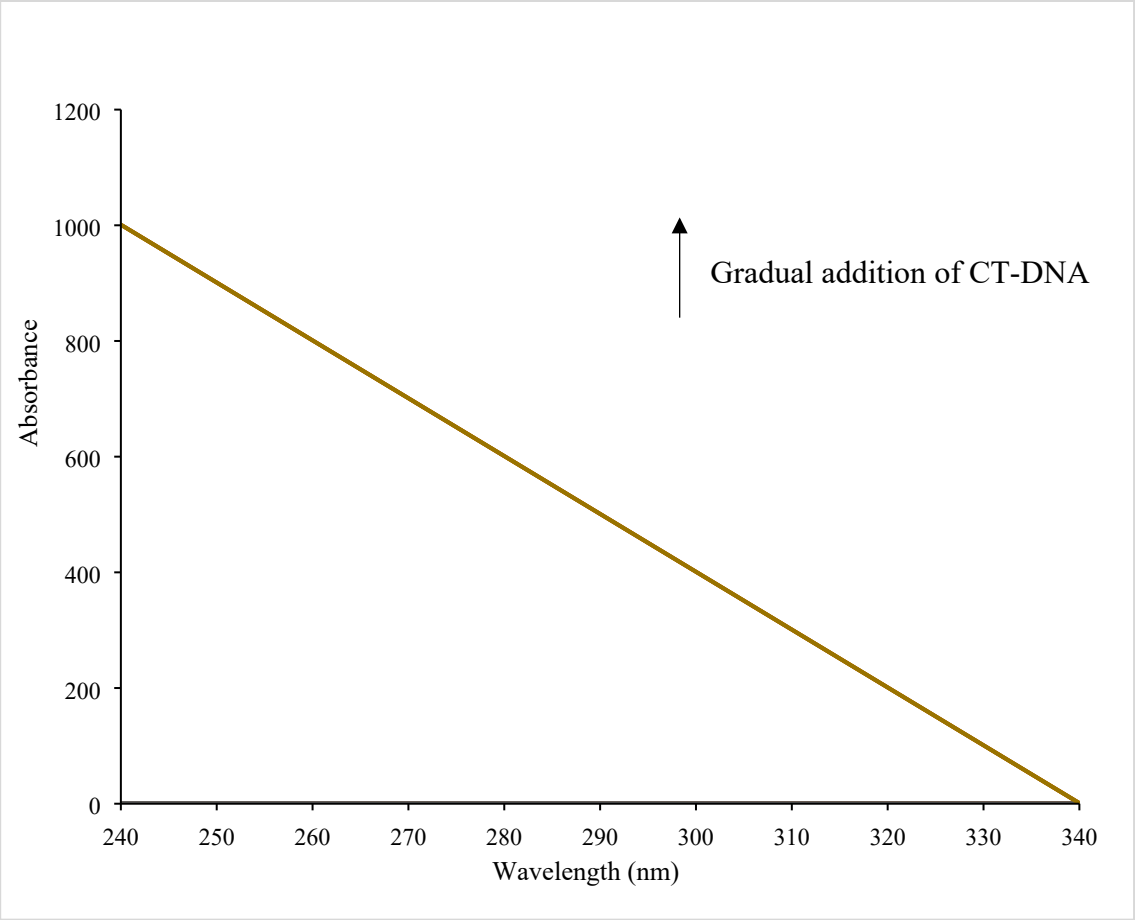

Fig. S10. Electronic absorption spectra of Re-CTZ-tmp in the absence (black line) and in the presence (color lines) of CT-DNA. The arrow shows the changes upon addition of increasing amount of CT-DNA. (C_{DNA} = 0-20 μM, $C_{complex}$ = 10 μM, samples prepared in DMSO/buffer Tris HCl medium, pH 7.4).

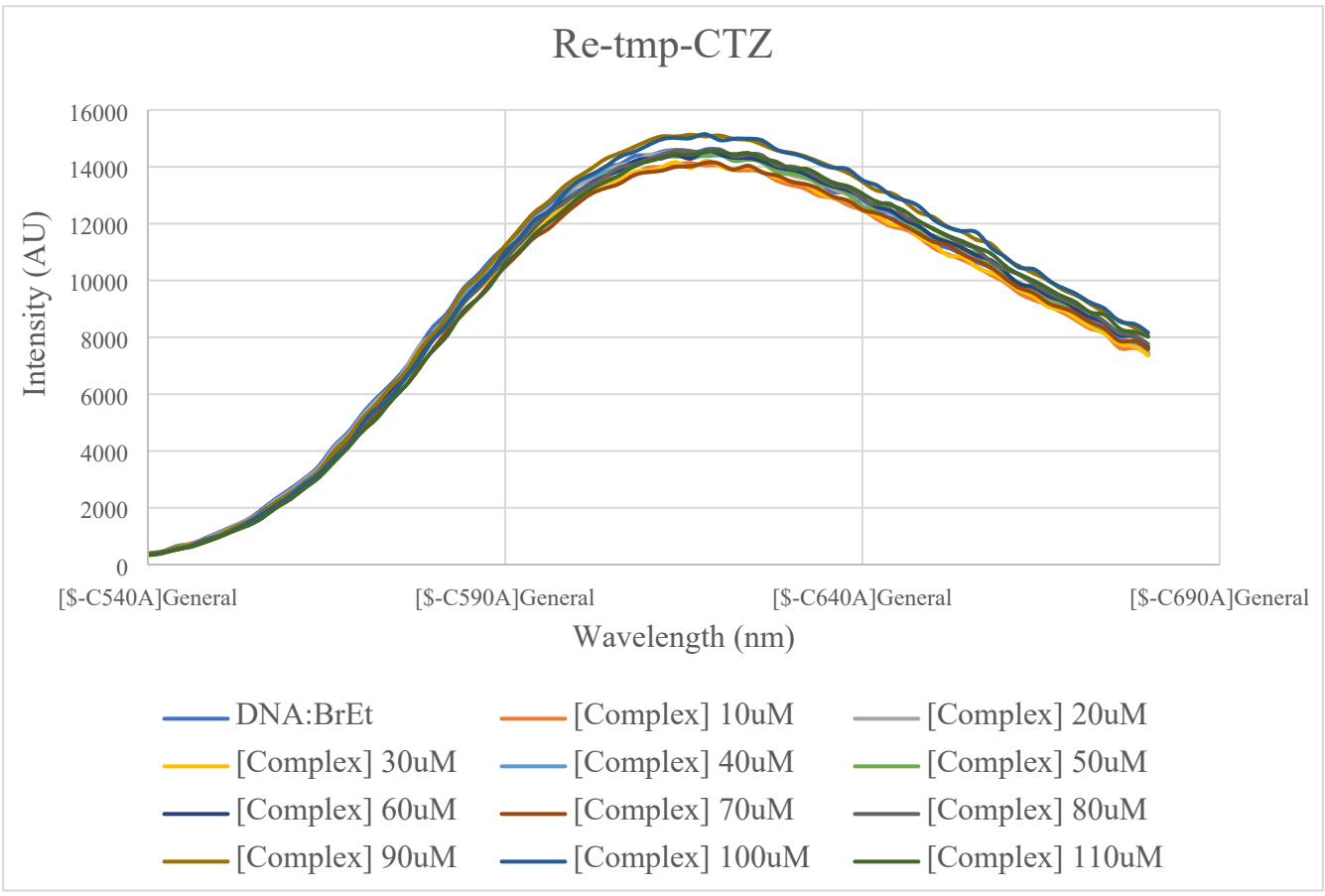

Fig. S11. Fluorescence data obtained for the competitive binding study of $[Re(CO)_3(tmp)(CTZ)]PF_6$ to {EB-DNA} adduct (λexc. = 510 nm).

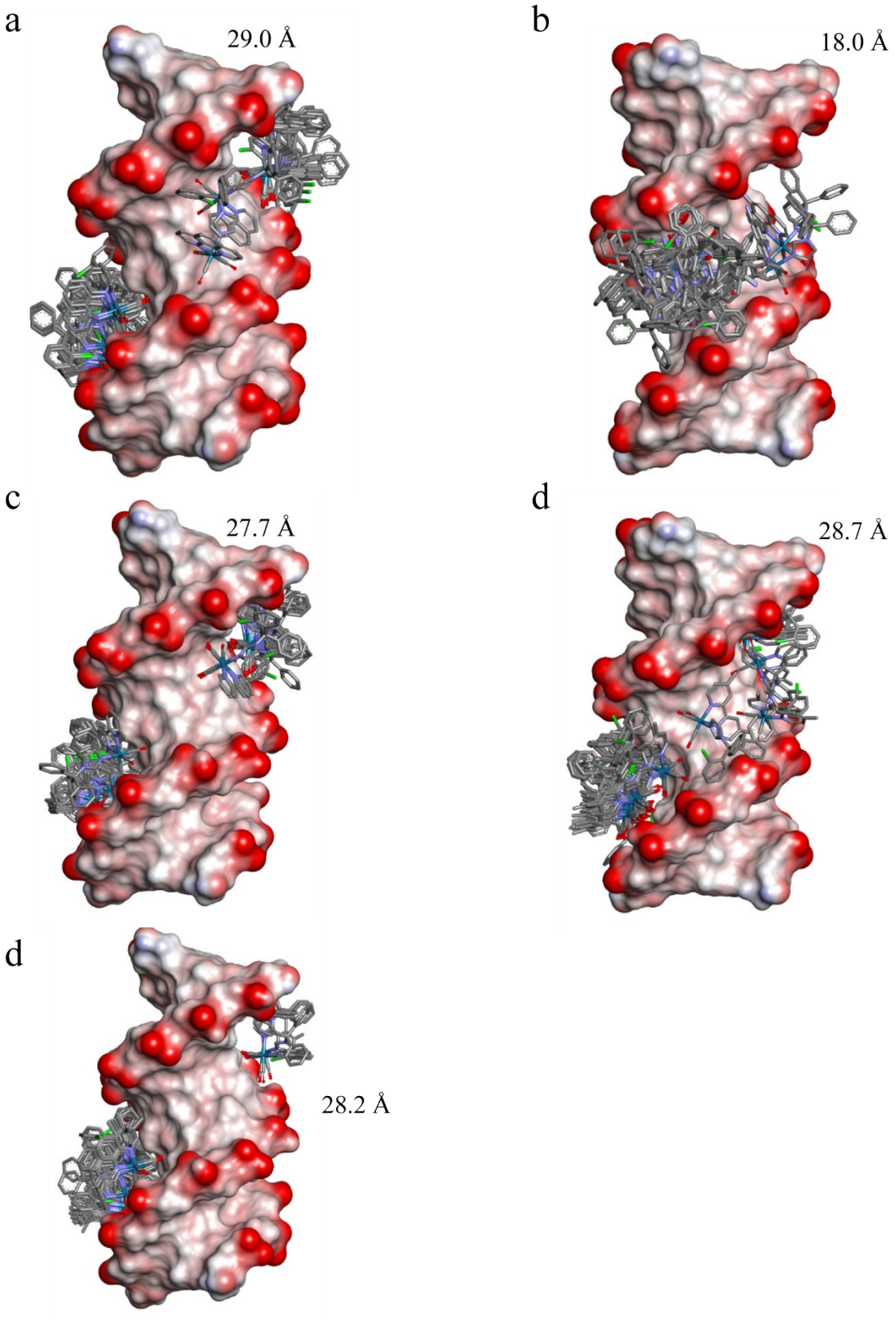

Fig. S12. Docking solutions for *fac*-[Re(I)(CO)$_3$(NN)(CTZ)]$^+$ using CT-DNA as receptor. NN = phen (a), aminophen (b), bipy (c), dmb (d), tmp (e). The solvent-accessible surface is depicted for the receptor,

with the interpolated atomic charges mapped on it. The RMSD between the solutions is also depicted. Atom color code: C (grey), N (blue), O (red), Cl (green), H (white).

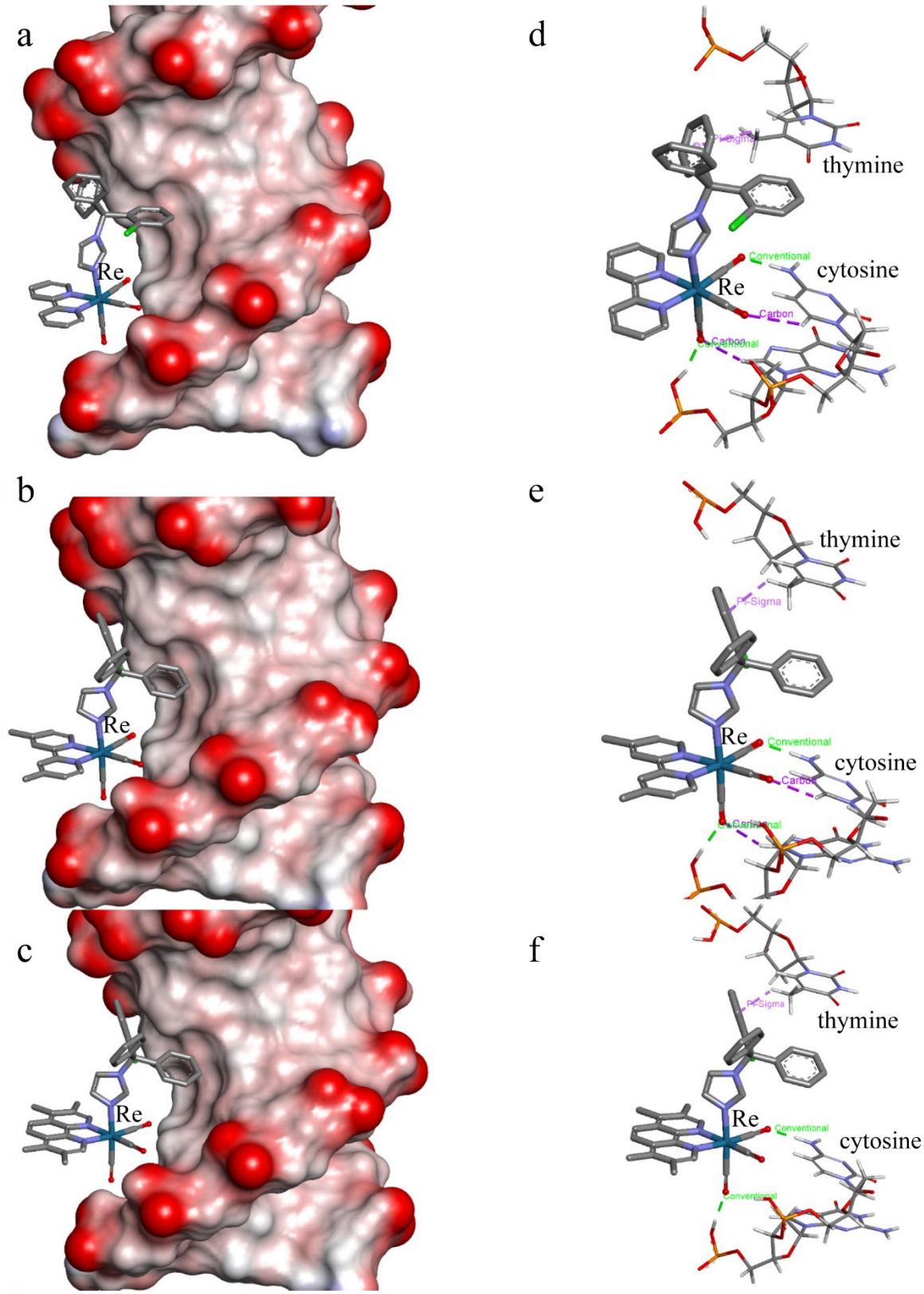

Fig. S13. Best ranking pose for *fac*-[Re(I)(CO)$_3$(NN)(CTZ)]$^+$ docked into the major groove of CT-DNA. NN = bipy (a), dmb (b), tmp (c). In all cases, the solvent-accessible surface is depicted for the receptor, with the interpolated atomic charges mapped on it. In (d) - (f), the intermolecular interactions between the substrate and the ct-DNA are shown for (a) - (c), respectively. Pi-sigma = C-H-π interaction;

conventional = conventional H-bond; Carbon = C-H H-bond. Atom color code: C (grey), N (blue), O (red), Cl (green), H (white).

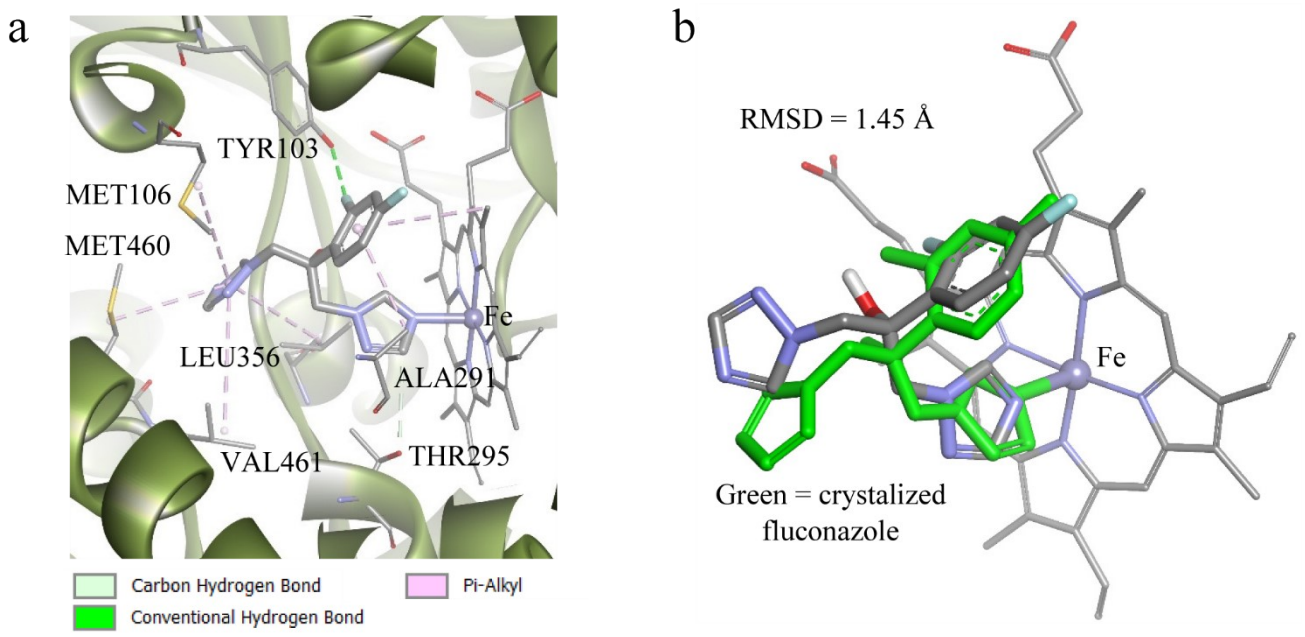

Fig. S14. a) Intermolecular interactions between the crystalized fluconazole and the receptor, represented as colored dashed lines. Atom color code: C (grey), N (blue), O (red), Cl (green), H (white). b) Redocking results for fluconazole. The crystallized fluconazole molecule is superimposed in green.